Terahertz Resonances of Transverse Standing Waves in a Corrugated Plate Waveguide

Jing Ma, Huan Liu, Shi-Yang Zhang, Wen-Li Zou, Ya-Xian Fan, and Zhi-Yong Tao

***Abstract*—Terahertz (THz) propagation in periodic structures has attracted great attention because of its captivating electrical and optical properties. However, the created THz band gaps are usually considered to be caused by Bragg resonances. Here, we theoretically and numerically investigate THz resonances and their related band gap properties in a periodically corrugated plate waveguide with arbitrary wall profiles. It has been found that the corrugated structure can cause not only the interaction between the same transverse modes, called the Bragg resonance, but also the strong interference between different transverse standing wave modes, which occurs in a higher frequency range with quite different features. Unlike the well-known Bragg resonance, the excited resonances between different transverse modes can produce the stronger energy attenuation and wider frequency band gap. The dispersion diagram is depicted to clearly describe the relationship between these resonances and waveguide geometries. Using this method, we can properly estimate the band gap structure of THz waveguides, which has been confirmed by the simulated results. In addition, these two resonances can be easily manipulated by changing the symmetry of waveguide structures. These findings on THz propagation in periodic waveguides could be applicable in high performance devices, such as filters, modulators and switches.**

***Index Terms*—Resonances, transverse standing-waves, periodic corrugation, band gaps.**

I. Introduction

TERAHERTZ (THz) wave refers to the special electromagnetic radiation between microwave and infrared light wave, which is just located in the transition region from macro electronics to micro photonics [1]–[5]. Due to the special frequency position, THz waves exhibits some unique advantages different from other frequency bands, such as perspective, transient, broadband and low radiation energy. So, THz technology has shown great application potentials in the fields of broadband communication [6]–[9], astronomical observation [10]–[12], biological imaging [13]–[15], nondestructive testing [16], [17], medical diagnosis [18], [19], and so on. At present, the research of THz technology is mainly devoted to the development of radiation sources, transmission technology, and functional devices with excellent performance. Among them, the THz waveguide transmission technology with low loss, long distance, and low dispersion is very essential due to the signal distortion in free space, the attenuation caused by atmospheric scattering, and the water vapor absorption. Various THz waveguides have been proposed and investigated, such as hollow metallic structures [20], metal wires [21], dielectric waveguides [22], parallel plate structures [23], photonic crystal fibers [24], [25], rectangular structures [26], plasmonic [27], and tapered waveguide [28]. However, most of researchers focused on the low loss and low dispersion THz waveguides and paid little attention to the transverse standing waves (i.e., the guided wave modes). Due to the lack of understanding on guided wave mode interaction, most waveguides only worked in a single-mode state. The realization of filtering, modulation, switching, and other functions mostly depends on new THz materials, such as two-dimensional materials and metamaterials [29]–[38]. Therefore, it is still a great challenge to develop waveguide devices that can effectively control THz waves.

Fortunately, periodic waveguide structure with intriguing band gap properties provides an effective way to solve this problem. Such artificial periodic materials are called photonic crystals in optics and has been widely used to develop a variety of optical [39] and THz devices [40], [41]. Most of these bandgaps were essentially identified as being caused by the well-known Bragg resonance, which originates from the strong interference between incident and reflected waves with the same transverse mode. It is worth noting that almost all researchers have focused on Bragg resonances, so the physical aspects far away from the Bragg frequency range is usually ignored, in which the standing wave coupling may occur. A few studies have predicted that there are not only Bragg resonances in the traditional sense in periodic waveguides, but also some unusual resonant phenomena, such as the so-called non-Bragg resonance [42] and Bloch resonance [43], and even sometimes, these resonances are mistaken for Bragg resonances. Unlike Bragg resonances, these unusual resonances are far away from the boundary of Brillouin zone, which is mainly induced by the interaction between different transverse modes in waveguides. In

Manuscript received March 16, 2022; revised April 19, 2022; accepted April 29, 2022. Date of publication May 3, 2022; date of current version May 17, 2022. This work was supported in part by the National Natural Science Foundation of China under Grants 12064005 and 62001132, in part by Guangxi Natural Science Foundation under Grants 2020GXNSFBA159047, 2021GXNSFAA220073, and 2021GXNSFDA075006, in part by Innovation Project of GUET Graduate Education under Grant 2022YCXS033, and in part by the Double First-class University Construction Project of Northwest University. *(Corresponding authors: Ya-Xian Fan and Zhi-Yong Tao.)*

Jing Ma and Wen-Li Zou are with the Institute of Modern Physics, Shaanxi Key Laboratory for Theoretical Physics Frontiers, Northwest University, Xi'an, Shaanxi 710127, China (e-mail: jingma900526@163.com; zouwl@nwu.edu.cn).

Huan Liu, Shi-Yang Zhang, Ya-Xian Fan, and Zhi-Yong Tao are with the Guangxi Key Laboratory of Wireless Wideband Communication and Signal Processing, Guilin University of Electronic Technology, Guilin 541004, China, and also with the Academy of Marine Information Technology, Guilin University of Electronic Technology, Beihai 536000, China (e-mail: huanliu@guet.edu.cn; 20022303167@mails.guet.edu.cn; yxfan@guet.edu.cn; zytao@guet.edu.cn).

Digital Object Identifier 10.1109/JPHOT.2022.3172059

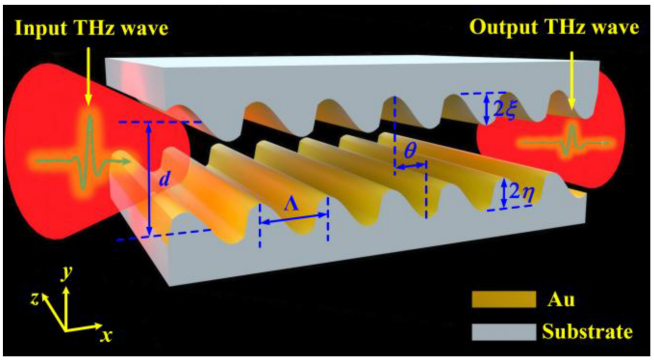

Fig. 1. Structural diagram of the proposed THz parallel plate waveguide structure with arbitrary periodically corrugations. The plate can be fabricated by coating a layer of gold film on a substrate. It is assumed that the structure extends infinitely along the z axis. The TE THz wave propagates along the x axis.

recent years, such resonances have been found and confirmed in acoustic cylindrical waveguides [44], water channels [45], [46], and even THz metal slits [47].

In this paper, we focus on the THz wave propagation far away from the Bragg resonant frequency in a periodically corrugated waveguide with arbitrary wall profiles. Another type of THz transverse standing-wave resonances is theoretically proposed and numerically confirmed in THz simulations. Different from the Bragg resonance, the standing-wave resonances occur away from the Brillouin edges and create a wider band gap, in which the energy attenuation is more intense. In the following section, we briefly describe the eigenvalue problem of THz waves in the periodic waveguide, and derive the generalized resonance conditions. The frequency band structures of different waveguide parameters are predicted by introducing the reference dispersion lines, which provide us a dispersion diagram method. We will find that the resonances of transverse standing waves always occur at the intersections of the reference lines, which clearly indicate the resonant interactions between THz waves and periodic waveguides. In Section III, the frequency band splitting is derived by calculating the Fourier integrals. The simulated dispersion curves and transmission spectra are shown to be in good agreement with the theoretical predictions. In Section IV, the electric field distribution and its mode analysis further confirm that the unusual resonant effect at higher frequencies are caused by the different transverse standing waves, which can be manipulated by the phase shift of the two plates. Finally, we summarize the main findings and briefly discuss their potential applications.

II. Resonances of Standing Waves

To clarify the physics of THz wave propagation in periodic waveguides, we present a THz waveguide resonance theory that takes into account the coupling between transverse standing waves and provides a complete description of wave propagation. Fig. 1 shows the proposed THz parallel plate waveguide with periodic corrugations. The waveguide consists of two plates with undulating structures. In order to effectively limit the propagation of THz waves in the waveguide, a layer of gold film is coated on the inner surface of the structure as a perfect electrical conductor. The gray and yellow areas in the figure represent the substrate and gold materials, respectively. The Cartesian coordinate system is also depicted at the left lower corner in Fig. 1 and the two plates are perpendicular to the y axis. θ is the phase shift between the upper and lower periodic corrugations and the two plates are symmetrical according to the xz plane when $\theta = 0$. The average distance between the two plate is d, whereas ξ, η, and Λ denote the two amplitudes and period length of corrugations, respectively. The corrugation amplitudes of the plates can be different while the period is the same. The THz waves are assumed to radiate along the x axis.

For TE waves with harmonic motion in time, the Helmholtz equation for the electric field intensity $\mathbf{E}$ in an ideal metal planar waveguide can be expressed as

$$\nabla^2\mathbf{E} + \frac{\omega^2}{c^2}\mathbf{E} = 0, \tag{1}$$

where $\omega = 2\pi f$ is the angular frequency and c is the speed of light in vacuum. And then, we can obtain the related boundary conditions in Cartesian coordinate system:

$$\mathbf{n} \times \mathbf{E} = 0, \text{on} \begin{cases} y_{up}(x) = \frac{d}{2}\left[1 + \xi W_{up}(Kx)\right], \\ y_{low}(x) = -\frac{d}{2}\left[1 - \eta W_{low}(Kx + \theta)\right]. \end{cases} \tag{2}$$

where $\mathbf{n}$ is the outward unit vector perpendicular to the boundary. The upper and low boundary are described by the periodic functions $W_{up}(Kx)$ and $W_{low}(Kx+\theta)$, respectively. $K = 2\pi/\Lambda$ is the wavenumber of waveguide corrugations and the spatial range between the plates can be expressed by $y_{up}(x)<y<y_{low}(x)$.

Since the undulating structure of the waveguide is periodically arranged along the x direction, it has little effect on the THz wave propagating along the z direction. Therefore, we can only consider the propagation characteristics of the electric field z component of TE waves E_z in our proposed periodic waveguide. Based on the Floquet theorem, E_z can be expanded as a spatial harmonic series

$$E_z = \sum_{n=-\infty}^{\infty} \left(a_n \cos k_{y,n} y + b_n \sin k_{y,n} y\right) \mathrm{e}^{\mathrm{i}k_{x,n}x}, \tag{3}$$

where a_n and b_n are the coefficients of different transverse standing waves, $k_{x,n} = \beta + nK$ and $k_{y,n}$ are the longitudinal and transverse wavenumber of the nth spatial harmonic, and β ($-K/2 \le \beta \le K/2$) is the reference propagation constant. Also, the dispersion relation is

$$\frac{\omega^2}{c^2} = k_{x,n}^2 + k_{y,n}^2. \tag{4}$$

By substituting Eq. (3) into the boundary condition (2), a system of linear algebraic equations with the coefficients $\mathbf{A} = \{a_n\}$ and $\mathbf{B} = \{b_n\}$ can be obtained by the Fourier integral transform, that is,

$$\mathbf{M} \cdot \begin{bmatrix} \mathbf{A} \\ \mathbf{B} \end{bmatrix} = 0, \text{with}, \mathbf{M} = \begin{bmatrix} C^{(+1)} & C^{(-1)} \\ C^{(+2)} & C^{(-2)} \end{bmatrix}, \tag{5}$$

where $\mathbf{M}$ is an $2m \times 2n$ matrix with

$$C_{mn}^{(+1)} = \int \frac{d}{2} \cos k_{y,n} \left[1 + \xi W_{up}(Kx)\right] \mathrm{e}^{-\mathrm{i}(m-n)Kx} \mathrm{d}x,$$

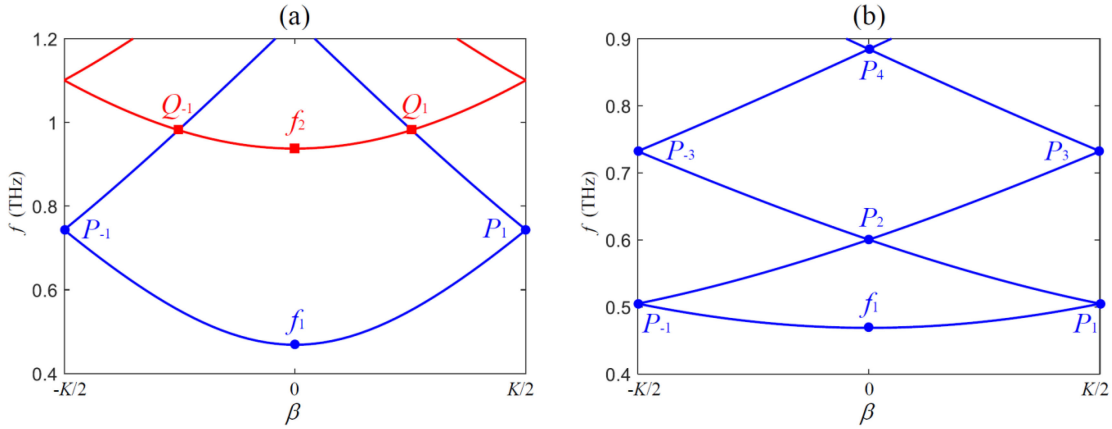

Fig. 2. References for dispersion curves in the first Brillouin zone: (a) Λ=260 μm and (b) Λ=800 μm. The blue and red lines represent the first and second transverse modes of different THz spatial harmonics, respectively.

$$C_{mn}^{(-1)} = \int \frac{d}{2} \sin k_{y,n} \left[1 + \xi W_{up}\left(Kx\right)\right] \mathrm{e}^{-\mathrm{i}(m-n)Kx} \mathrm{d}x,$$
$$C_{mn}^{(+2)} = -\int \frac{d}{2} \cos k_{y,n} \left[1 - \eta W_{low}\left(Kx+\theta\right)\right] \mathrm{e}^{-\mathrm{i}(m-n)Kx} \mathrm{d}x,$$
$$C_{mn}^{(-2)} = -\int \frac{d}{2} \sin k_{y,n} \left[1 - \eta W_{low}\left(Kx+\theta\right)\right] \mathrm{e}^{-\mathrm{i}(m-n)Kx} \mathrm{d}x. \tag{6}$$

In order to obtain the nontrivial solutions of a_n and b_n, it is required that the determinant of the matrix $\mathbf{M}$ must be zero, i.e.,

$$\det \left|\left|\mathbf{M}\left(k_{y,n}, \beta; \xi, \eta, K, \theta\right)\right|\right| = 0 \tag{7}$$

For a fixed frequency ω, we can derive the relation between the transverse wavenumbers of the nth and the n'th harmonics according to the dispersion relation (4):

$$k_{y,n} = \sqrt{k_{y,n'^2} + 2(n'-n)K\beta + (n'^2 - n^2)K^2}. \tag{8}$$

If $\eta = \xi = 0$, we can obtain the solution of Eq. (7), which is $k_{y,0} = k_y^{(p)}/d$. The different values of $k_y^{(p)}$ correspond to different transverse standing wave modes, i.e., $\{k_y^{(p)}, p = 1, 2, 3, \ldots\} = \{\pi, 2\pi, 3\pi, \ldots\}$ for TE waves. The THz wave resonance between the nth and n'th harmonics occurs at

$$\beta_{pq} = -\frac{(n+n')K}{2}(1 + g_{pq}), \text{ with } g_{pq} = \frac{k_y^{(q)^2} - k_y^{(p)^2}}{(n'^2 - n^2)K^2 d^2}. \tag{9}$$

When $p = q$, the nth and n'th harmonics have the same transverse mode, which will cause the well-known Bragg resonance at $\beta_{pq} = -(n+n')K/2$. Otherwise ($p \neq q$), some unusual resonances will happen, such as the so-called non-Bragg resonance [42]. Thus, the frequency of the generalized resonance between the pth mode of the nth harmonic and the qth mode of the n'th harmonic can be expressed as

$$f_{pq} = \frac{c}{2\pi}\sqrt{\frac{k_y^{(p)^2}}{d^2} + (\beta_{pq} + nK)^2} = \frac{c}{2\pi}\sqrt{\frac{k_y^{(q)^2}}{d^2} + (\beta_{pq} + n'K)^2}. \tag{10}$$

Since the transverse wavenumber $k_y^{(p)}$ takes the fixed discrete value, the resonant frequency only depends on the average distance d and the wavenumber of corrugation K, which means we can manipulate the resonances by selecting the corrugation geometries.

To further investigate and intuitively display the THz resonance and band gap properties of the corrugated waveguide, according to the dispersion relation (4), we propose a dispersion diagram by depicting the reference for dispersion curves in the first Brillouin zone in Fig. 2 with some marked special points for $d = 320$ μm. They are the cut-off frequencies of the first- and the second-mode f_1, and f_2, and the intersections $P_{\pm1}$, $Q_{\pm1}$, P_2, $P_{\pm3}$, P_4. The blue and red lines denote the first and second transverse standing wave modes, respectively, while P_i and Q_i are the intersections of the same and different modes. Fig. 2(a) shows the dispersion diagram for $\Lambda = 260$ μm. We can see that the two curves with the same color intersect at points P_{-1} and P_{+1} and these two intersections are just at the boundary of Brillouin zone. We firmly believe that the two spatial harmonics with the same transverse mode will produce strong interference near the frequency point of the intersection, resulting in the frequency domain band gap, which is the well-known Bragg resonance phenomenon. At this time, only one Bragg resonance can be observed in the frequency range lower than the cut-off frequency of the second-order mode f_2. However, in addition to the Bragg resonance, the resonance interaction between different modes can also occur, that is, points Q_{-1} and Q_{+1} where the blue and red curves intersect. These points are located at higher frequencies and far away from the boundary of the Brillouin zone. We predict that this unusual resonance of transverse standing waves can also cause the spectral band splitting and the possible frequency band gap.

In Fig. 2(a), the positions of points P_{-1} and P_{+1} are closely related to the period of the waveguide, while points f_1 and f_2 do not. With the increase of period length, these two points P_{-1} and P_{+1} gradually move down, and then more and more first-order modes are involved. So, the multiple order Bragg resonances can occur. When the period length increases to a certain extent, only the high-order spatial harmonics can intersect the red line. Therefore, the resonance of different transverse standing waves at high frequency is too small to be excited and only the Bragg resonances can happen. Fig. 2(b) shows the references of the

guided wave modes for $\Lambda = 800\ \mu$m. Clearly, P_{-1} and P_{+1} move towards the low frequency and point P_2 is far away from the second-mode cut-off. There are four Bragg resonances $P_{\pm1}$, P_2, $P_{\pm3}$, and P_4 appearing at the intersections of the blue lines. Here, it should be emphasized that by using the proposed dispersion diagram, we can approximately estimate the frequency band structure of the periodic waveguide. More importantly, when a specific band structure is required in practical applications, this method can help us to design the geometry parameters of waveguides and accurately guide the preparation of THz functional devices.

III. Resonance Induced Band Gaps

Assuming that the corrugation shape of the upper and lower plates in the waveguide is cosine, that is, $W_{up} = \cos(Kx)$ and $W_{low} = \cos(Kx+\theta)$, and then substitute them into Eq. (6), we can calculate the Fourier integrals and obtain

$$\begin{aligned}
C_{mn}^{(+1)} &= \mathrm{J}_{|m-n|}\left(\frac{d\xi k_{y,n}}{2}\right)\cos\frac{\pi\,|m-n|+dk_{y,n}}{2},\\
C_{mn}^{(-1)} &= \mathrm{J}_{|m-n|}\left(\frac{d\xi k_{y,n}}{2}\right)\sin\frac{\pi\,|m-n|+dk_{y,n}}{2},\\
C_{mn}^{(+2)} &= -\mathrm{J}_{|m-n|}\left(\frac{d\eta k_{y,n}}{2}\right)\cos\frac{\pi\,|m-n|+dk_{y,n}}{2}\mathrm{e}^{\mathrm{i}(m-n)\theta},\\
C_{mn}^{(-2)} &= \mathrm{J}_{|m-n|}\left(\frac{d\eta k_{y,n}}{2}\right)\sin\frac{\pi\,|m-n|+dk_{y,n}}{2}\mathrm{e}^{\mathrm{i}(m-n)\theta},
\end{aligned} \tag{11}$$

where $\mathrm{J}_{|m-n|}(\cdot)$ is the $|m\text{-}n|$th order Bessel function. Near the resonance of $n = 0, 1$, Eq. (7) reduces to

$$\begin{aligned}
\tan(k_{y,0}d)\tan(k_{y,1}d) = \frac{1}{16}d^2k_{y,0}k_{y,1}\left[\eta^2+\xi^2\right.\\
\left.+2\eta\xi\cos\theta\sec(k_{y,0}d)\sec(k_{y,1}d)\right]
\end{aligned} \tag{12}$$

For the same order small ξ and η, we have the expansion,

$$k_{y,0} = k_y^{(p)} + \delta k\cdot\xi, \tag{13}$$

in terms of ξ and η, with

$$\delta k = \pm\frac{k_y^{(q)}}{4d}\sqrt{1+\gamma^2+2\gamma\cos\theta\sec dk_y^{(p)}\sec dk_y^{(q)}}, \tag{14}$$

where $\gamma{=}\eta/\xi$. And then the frequency spectrum splits:

$$f_{pq}^{\pm} = f_{pq} \pm \frac{f_p}{f_{pq}}\frac{c}{2\pi}\,|\delta k|\cdot\xi, \tag{15}$$

where

$$f_p = \frac{ck_y^{(p)}}{2\pi d}, \tag{16}$$

is the cut-off frequency of the pth transverse standing wave mode. The resonant interaction between the transverse standing-waves leads to the frequency shifts of f_{pq} and the generation of f_{pq}^{-} and f_{pq}^{+}, which are located away from the resonant frequency. So, the bandwidth Δf can be easily obtained, i.e.,

$$\Delta f = \frac{f_p}{f_{pq}}\frac{c}{\pi}\,|\delta k|\cdot\xi. \tag{17}$$

It can be found that the frequency splitting results in the band gap with the width proportional to ξ. The larger the corrugation amplitude, the wider is the created band gap. The assumption of the cosine wall profile can lead to the analytical solution while the numerical solution can be achieved for the other wall profiles.

Generally, the periodic corrugation of the parallel plate waveguide can lead to the resonances between different transverse standing waves and the created band gap is proportional to the corrugation amplitude. We can select the waveguide geometry to efficiently engineering the spectral band structure of THz radiation.

To better understand the relationship between the band gap structure and geometric parameters of the waveguide, the numerical simulation was employed to investigate the dispersion and attenuation properties of THz waveguides by using the COMSOL Multiphysics software. Based on the finite element method (FEM) the dispersion curves and corresponding transmission spectrum were simulated with different geometries. For convenience and reduction of drawing error, the corrugated shape was selected as a rectangular. The corrugation amplitudes of the upper and lower plates $\xi = \eta = 40\ \mu$m, the phase shift $\theta{=}\pi/2$, and the average distance $d = 320\ \mu$m. The number of periods was set to 10. The transmission medium in the waveguide was the air. To limit the propagation of THz waves in the waveguide, the corrugated profile was applied as the perfect electrical conductor boundary. To ensure the accuracy of the simulation results, the ultra-fine grids were adopted and the frequency step was set to be 0.001 THz.

Fig. 3 shows the simulated dispersion curves and transmission spectra of THz periodic waveguides with rectangular corrugated boundaries. For $\Lambda = 260\ \mu$m in Fig. 3(a) and (b), the simulated results agree well with the theoretical predictions in Fig. 2(a). We can see that the Bragg resonance of the same modes appears in the range of 0.73–0.79 THz, which is just located at the boundary of the first Brillouin zone with $\beta = \pm K/2$. When the resonance occurs, the dispersion curves break off, which means that THz waves cannot propagate through the waveguide at the breaking point. As expected, an obvious stop band A_1 can be observed at the corresponding frequency range in the transmission spectrum with smooth band edges. Therefore, the resonance at point $P_{\pm1}$ with Bragg nature can be easily identified.

Besides that, another type of resonances appears in the higher frequency range, which is indicated by the breaking of the dispersion curves far away from the edges of the first Brillouin zone. Similar to the Bragg resonances, the dispersion curve breaking can also lead to the frequency band splitting and the creation of forbidden band B_1 as shown in Fig. 3(b). For the half of the maximum transmission, i.e., 0.5, the widths of band gaps A_1 and B_1 are 0.027 THz and 0.041 THz, respectively. It should be noted that such different resonances can lead to the stronger energy attenuation and wider frequency band gap around 1.0 THz, and the edges of the stop band induced by different transverse standing waves are much steeper. The

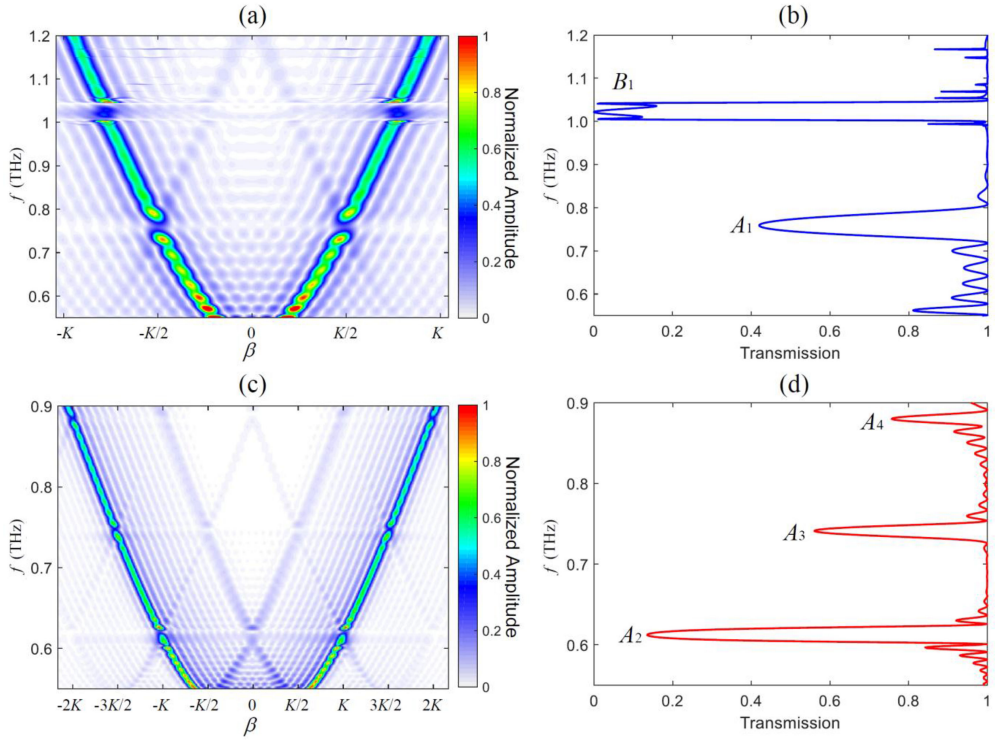

Fig. 3. Simulated dispersion curves and transmission spectra of THz periodic waveguides with rectangularly corrugated boundaries: (a) and (b) Λ=260 μm, (c) and (d) Λ=800 μm.

simulation results are basically consistent with the theoretical prediction in Fig. 2(a). This unique band gap property is very important for the design of THz waveguide devices with excellent performance.

Fig. 3(c) and (d) show the simulated dispersion curves and transmission spectra for $\Lambda = 800$ μm, respectively. Referring to the theoretical prediction results in Fig. 2(b), we do observe the multiple order resonances and their induced stop bands in the similar frequency range. The dispersion curves in Fig. 3(c) break off around 0.6 THz, 0.75 THz, and 0.9 THz with $\beta = \pm K$, $\beta = \pm 3K/2$, and $\beta = \pm 2K$, respectively, which are located at the boundaries of the Brillouin zones. It also could be found that the breaks get smaller when the frequency increases, indicating the weaker resonant intensity. Moreover, in Fig. 3(d), the band edges are relatively smooth, and the bandwidth gradually decreases with the increasing frequency. Therefore, these resonances can be recognized as the Bragg resonances with different orders. Here, it needs to be explained that the theoretically predicted Bragg resonance P_1 in Fig. 2(b) does not appear in the transmission spectrum. This is because that the average distance d of the waveguide remains unchanged during the simulation, and the introduced undulated structure reduces the nearest distance, so that the cut-off frequency moves up and masks the first-order Bragg resonance.

The simulated dispersion curves confirm the theoretical predictions of the proposed dispersion diagram in Section II. All the breaks of dispersion curves appear at the intersections of the reference lines, which indicate the resonances of the transverse standing waves. As predicted, the Bragg resonances induced by the interference of the same transverse standing waves occur at the edges of the Brillouin zones while the resonances of different transverse standing waves happen away from the edges. Both types of resonances can result in the forbidden bands and the band gap decreases with the increasing resonant order. Furthermore, the resonances of different transverse standing waves not only occur in the middle of the Brillouin zone, but also create the band gap with quite different properties, which can cause the more efficient wave attenuation than the traditional Bragg resonances. It means that the smaller structure can achieve the same effects on THz wave attenuation or reflection when the resonances of different transverse standing waves are employed in applications.

IV. Transverse Standing Waves and Band Gap Manipulation

In the first two parts, we have presented a complete theoretical analysis and numerical simulation for the propagation of THz wave in the periodic corrugated parallel plate waveguide. Combined with the reference lines and the dispersion curves, we also have demonstrated how the THz resonances in a periodic waveguide depends on the corrugated period and how the resonances of different transverse standing waves occur in the middle of the first Brillouin zone. The resonances with different properties do create the different band gaps. The different transverse standing wave resonance is more intense and leads to the more efficient wave attenuation. This unique property is supposed to be related to the transverse standing waves of THz waveguides. It seems that the different standing wave interactions are more intense and effective.

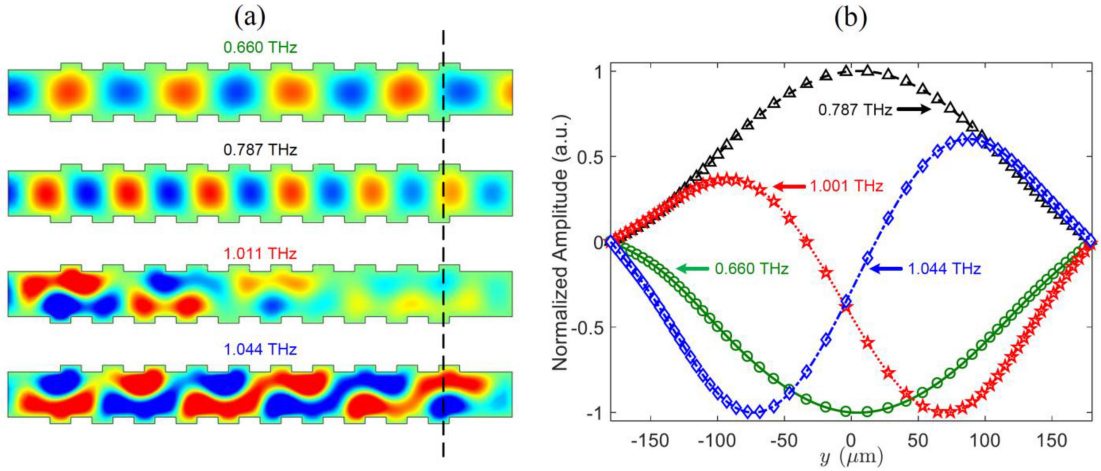

Fig. 4. (a) Simulated electric field distribution of E_z component at frequencies 0.660, 0.787, 1.011 and 1.044 THz for Λ=260 μm. The dashed line indicates the location of the transverse field distribution for the further analysis. (b) Mode fitting curves corresponding to the electric field along y axis near the outlet. All the E_z components are normalized by the maxima of their own data set.

To better understand the THz resonance of transverse standing waves in the corrugated plate waveguide, we have applied the FEM to simulate the electric field distribution for $\Lambda = 260$ μm at several frequencies, and some of them are shown in Fig. 4(a). First two figures for 0.660 THz and 0.787 THz show the wave propagation below and within the Bragg gap A_1, respectively. Clearly, the simulated electric field is symmetrically distributed with respect to the x-axis, which exhibits the first transverse standing wave propagation and attenuation along the waveguide. Unlike the Bragg gap, for band gap B_1 at the higher frequencies of 1.001 THz and 1.044 THz, the second-order mode of transverse standing wave patterns is involved, and it causes a stronger interaction with the first-order mode, resulting in an antisymmetric electric field as shown in the last two figures in Fig. 4(a). The obvious difference between band gap A_1 and B_1 in the electric field distributions helps us to understand the propagation of THz waves in periodic waveguides more deeply. They also demonstrate the unique characteristics of the different standing wave resonance.

To further confirm the standing wave mode components of gaps A_1 and B_1, we have also performed the mode fitting on the electric fields along the y axis near the outlet by a truncated model

$$E_z(y) = a_1 \cos\frac{\pi y}{D} + b_2 \sin\frac{2\pi y}{D} + a_3 \cos\frac{3\pi y}{D} + b_4 \sin\frac{4\pi y}{D}, \tag{18}$$

with the maximum distance $D = 360$ μm as shown in Fig. 4(b). In the model, a_1, b_2, a_3 and b_4 represent fitting coefficients of the first four transverse standing wave modes, with $a_1+b_2+a_3+b_4 = 1$. The position marked by the black dashed line in Fig. 4(a) shows the selected electric field distribution near the outlet. For convenience, the y direction field distributions at 0.660 THz, 0.787 THz, 1.011 THz, and 1.044 THz are normalized by their own maxima and shown in Fig. 4(b) by the circles, triangles, stars, and diamonds, respectively. The best fitting curve for 0.787 THz within the Bragg gap A_1 is shown by the black dashed line in Fig. 4(b), the percentages of optimal fitting coefficients are $a_1 = 88.27\%$, $b_2 = 4.19\%$, $a_3 = 6.70\%$, and $b_4 = 0.84\%$, and the root mean square error (RMSE) $\sigma = 0.003671$, with 95% confidence bounds. It means that the first-order standing wave mode is the main component and the higher-order modes are puny, which further confirms the resonance with Bragg nature. The blue dash-dot line represents the best fitting curve for 1.044 THz within gap B_1, the percentages of optimal fitting coefficients are $a_1 = 23.12\%$, $b_2 = 66.04\%$, $a_3 = 2.53\%$, and $b_4 = 8.32\%$, and the RMSE $\sigma = 0.003686$, with 95% confidence bounds. Obviously, the first- and the second-order standing wave modes are dominant as expected, indicating that the first two modes are involved in the resonances. The simulation results on electric fields firmly confirm the above theoretical analysis. The unique properties of gap B_1 are attributed to the first and second transverse standing wave resonances.

The mode component fitting method further demonstrate the THz resonances of transverse standing waves. The resonances occurring at the edges of the Brillouin zones are caused by the interference between the same transverse standing waves while the other type of resonances in the middle of the Brillouin zone is involved by the different transverse standing waves, which can create the much wider gap and much stronger attenuation. The mode components of the other two cases at 0.660 THz and 1.011 THz are very similar, and therefore are not discussed here to avoid repetition.

Based on the previous analysis, we have known that the period length of THz waveguides has a great influence on the band gap structure, but the phase shift θ is fixed to $\pi/2$ in the whole analysis, which can also effect on the propagation characteristics of THz waves in another way. Fig. 5(a) shows the simulated frequency dependent THz transmission spectra for $\theta = 0$ and π by the blue dotted and red dash-dot lines, respectively. The period length is fixed to 260 μm. Interestingly, when the phase shift $\theta = 0$, that is, the corrugations of the two plates are symmetrical with respect to the x-axis, only Bragg gap A_1 can be found. On the contrary, when the phase shift θ increases to π, the upper and lower grooves are completely staggered, and the former symmetry of the waveguide structure is broken. At this time, the Bragg gap of the same transverse standing

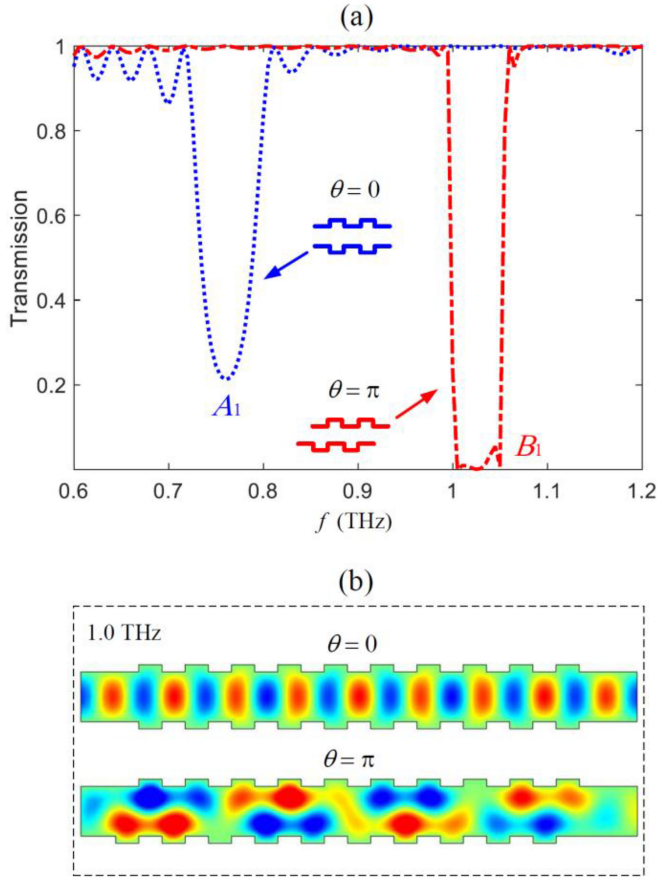

Fig. 5. (a) Simulated THz transmission spectra vs frequency for θ=0 (the dotted line) and π (the dash-dot line). The insets indicate the geometry of the waveguides in the both cases and the two types of gaps appear alternately. (b) Simulated electric field distribution of E_z component at 1.0 THz for different phase shifts.

waves disappears whereas the resonance induced gap of different transverse modes B_1 appears. In the different waveguides, the band widths of A_1 and B_1 are similar, but the attenuation is still much stronger in gap B_1. By selecting the geometry parameter of phase shift θ, we can manipulate the band gaps by creating only one (A_1/B_1) or both two (A_1 and B_1) gaps. This controllable band structure could be applied to design the more effective and efficient THz devices.

In addition, the phase shift can also affect the transverse standing wave propagating through the waveguide as shown in Fig. 5(b). At 1.0 THz, the THz waves are in the pass bands of waveguides with $\theta = 0$ and $\theta = \pi$, but the propagating modes are different. It is clear that there is only the first-order standing wave mode when $\theta = 0$ because of the symmetric structure and the incident first-order mode. When $\theta = \pi$, the structure is totally antisymmetric. Although there still only the first-order mode excited, it changes to the antisymmetric second-order mode in the pass band due to the structural symmetry. Since the first- and second-modes have been analyzed, the similar mode component analysis of propagating transverse standing waves is not included.

In applications, it could be a challenge to adjust phase shift between the two corrugated plates. The one-side grooved waveguide can be considered, which consists of one grooved plate and one planar plate. Its characteristics of dispersion curves and transmission spectrum are very similar to these of the two-side grooved waveguide with $\theta = \pi/2$ as shown in Fig. 3(a) and (b), respectively. Due to the absence of one-side corrugation, the resonant intense decreases, but the different transverse standing wave resonances can be also found.

V. Conclusion

In conclusion, we have performed both theoretical and numerical investigations on THz wave propagation in a parallel plate waveguide with arbitrary periodically corrugated structures and explored the existence of another type of THz resonances $Q_{\pm 1}$ in addition to the well-known Bragg resonance. By using the theoretical analysis and the dispersion diagram in the first Brillouin zone, we predict the band structure of THz waveguides and find that it highly depends on the period length. The numerical simulations based on the FEM are employed to analyze the resonance-induced band gaps. Both Bragg resonance $P_{\pm 1}$ and the resonance of different transverse standing wave mode $Q_{\pm 1}$ are predicted theoretically and then confirmed by the simulations. Obviously different from Bragg resonances, the resonance $Q_{\pm 1}$ is caused by the strong interference between different transverse standing waves, which makes itself occur in the higher frequency range. In addition, both band gaps are highly tunable by the phase shift θ between the upper and lower plates of the waveguide. The simulated electric field distribution and mode fitting have further confirmed that the physical mechanism of the two resonances is completely different. Unexpectedly, compared with Bragg gap A_1, the observed gap B_1 is impressively wide, and the transmission loss inside this gap is much greater, indicating that the Q_1 resonance can plays a more essential role in the propagation of THz waves in such periodic waveguides. The present work provides a detailed physical picture for the propagation and interaction of standing waves in planar THz waveguides. All these theoretical findings could pave the way to the design of more effective THz waveguide devices, such as filters, modulators, and switches.

References

[1] B. Ferguson and X. C. Zhang, "Materials for terahertz science and technology," *Nat. Mater.*, vol. 1, no. 1, pp. 26–33, Sep. 2002.
[2] P. H. Siegel, "Terahertz technology," *IEEE Trans. Microw. Theory Tech.*, vol. 50, no. 3, pp. 910–928, Mar. 2002.
[3] P. H. Siegel, "Terahertz technology in biology and medicine," *IEEE Trans. Microw. Theory Tech.*, vol. 52, no. 10, pp. 2438–2447, Oct. 2004.
[4] M. Tonouchi, "Cutting-edge terahertz technology," *Nat. Photon.*, vol. 1, no. 2, pp. 197–105, Feb. 2007.
[5] D. M. Mittleman, "Frontiers in terahertz sources and plasmonics," *Nat. Photon.*, vol. 7, no. 9, pp. 666–669, Sep. 2013.
[6] S. Koenig *et al.*, "Wireless sub-THz communication system with high data rate," *Nat. Photon.*, vol. 7, no. 12, pp. 977–981, Dec. 2013.
[7] T. Nagatsuma, G. Ducournau, and C. C. Renaud, "Advances in terahertz communications accelerated by photonics," *Nat. Photon.*, vol. 10, no. 6, pp. 371–379, Jun. 2016.
[8] H. J. Song and T. Nagatsuma, "Present and future of terahertz communications," *IEEE Trans. Tera. Sci. Tech.*, vol. 1, no. 1, pp. 256–263, Sep. 2011.

[9] J. Federici and L. Moeller, "Review of terahertz and sub-terahertz wireless communications," *J. Appl. Phys.*, vol. 107, 2010, Art. no. 111101.

[10] C. Kulesa, "Terahertz spectroscopy for astronomy: From comets to cosmology," *IEEE Trans. Tera. Sci. Tech.*, vol. 1, no. 1, pp. 232–240, Sep. 2011.

[11] W. D. Langer, T. Velusamy, and H. W. Yorke, "C^+ detection of warm dark gas in diffuse clouds," *Astron. Astrophys*, vol. 521, 2010, Art. no. L17.

[12] D. V. Meledin, "A 1-THz superconducting hot-electron-bolometer receiver for astronomical observations," *IEEE Trans. Microw. Theory Tech.*, vol. 52, no. 10, pp. 2338–2343, Oct. 2004.

[13] H. Lindley-Hatcher *et al.*, "Real time THz imaging-opportunities and challenges for skin cancer detection," *Appl. Phys. Lett.*, vol. 118, 2021, Art. no. 230501.

[14] H. Hoshina *et al.*, "Terahertz pulsed imaging of frozen biological tissues," *Appl. Phys. Lett.*, vol. 94, 2009, Art. no. 123901.

[15] A. Wojdyla and G. Gallot, "Attenuated internal reflection terahertz imaging," *Opt. Lett.*, vol. 38, no. 2, pp. 112–114, Jan. 2013.

[16] C. D. Stoik, M. J. Bohn, and J. L. Blackshire, "Nondestructive evaluation of aircraft composites using transmissive terahertz time domain spectroscopy," *Opt. Exp.*, vol. 16, no. 21, pp. 17039–17051, Oct. 2008.

[17] Y. C. Shen and P. F. Taday, "Development and application of terahertz pulsed imaging for nondestructive inspection of pharmaceutical tablet," *IEEE J. Sel. Top. Quant. Electron.*, vol. 14, no. 2, pp. 407–415, Mar./Apr. 2008.

[18] R. M. Woodward *et al.*, "Terahertz pulse imaging in reflection geometry of human skin cancer and skin tissue," *Phys. Med. Biol.*, vol. 47, no. 21, pp. 3853–3863, Nov. 2002.

[19] R. M. Woodward *et al.*, "Terahertz pulse imaging of ex vivo basal cell carcinoma," *J. Invest. Dermatol.*, vol. 120, no. 1, pp. 72–78, Jan. 2003.

[20] G. Gallot, S. P. Jamison, R. W. McGowan, and D. Grischkowsky, "Terahertz waveguides," *J. Opt. Soc. Amer. B*, vol. 17, no. 5, pp. 851–863, May 2000.

[21] K. Wang and D. M. Mittleman, "Metal wires for terahertz wave guiding," *Nature*, vol. 432, no. 7015, pp. 376–379, Nov. 2004.

[22] H. Amarloo and S. Safavi-Naeini, "Enhanced on-chip terahertz vibrational absorption spectroscopy using evanescent fields in silicon waveguide structures," *Opt. Exp.*, vol. 29, no. 11, pp. 17343–17352, May 2021.

[23] K. Dhriti *et al.*, "Plasmon-induced transparency in an air-dielectric grooved parallel-plate terahertz waveguide," *J. Opt. Soc. Amer. B*, vol. 38, no. 4, pp. 1290–1296, Apr. 2021.

[24] D. K. Lu *et al.*, "Photonic bandgap terahertz fibers based on honeycombed tubes," *Opt. Exp.*, vol. 29, no. 26, pp. 43516–43530, Dec. 2021.

[25] J. Webber *et al.*, "Terahertz band communications with topological valley photonic crystal waveguide," *J. Lightw. Technol.*, vol. 39, no. 24, pp. 7609–7620, Dec. 2021.

[26] V. Georgiadis *et al.*, "Dispersion in dielectric-lined waveguides designed for terahertz-driven deflection of electron beams," *Appl. Phys. Lett.*, vol. 118, no. 14, 2021, Art. no. 144102.

[27] C. C. Huang *et al.*, "Terahertz hybrid plasmonic waveguides with ultra-long propagation lengths based on multilayer graphene-dielectric stacks," *Opt. Exp.*, vol. 29, no. 24, pp. 39521–39535, Nov. 2021.

[28] G. Balistreri *et al.*, "Time-domain integration of broadband terahertz pulses in a tapered two-wire waveguide," *Laser Photon. Rev.*, vol. 15, no. 8, 2021, Art. no. 2100051.

[29] W. B. He *et al.*, "Ultrafast all-optical terahertz modulation based on an inverse-designed metasurface," *Photon. Res.*, vol. 9, no. 6, pp. 1099–1108 2021.

[30] W. W. Liu and Z. Y. Song, "Terahertz absorption modulator with largely tunable bandwidth and intensity," *Carbon*, vol. 174, pp. 617–624, Apr. 2021.

[31] Q. H. Wang *et al.*, "Design, fabrication, and modulation of THz bandpass metamaterials," *Laser Photon. Rev.*, vol. 13, 2019, Art. no. 1900071.

[32] S. Kovalev *et al.*, "Electrical tunability of terahertz nonlinearity in graphene," *Sci. Adv.*, vol. 7, 2021, Art. no. eabf9809.

[33] S. Zheng *et al.*, "Terahertz transmissive metasurface for realizing beam steering by frequency scanning," *J. Lightw. Technol.*, vol. 39, no. 17, pp. 5502–5507, Sep. 2021.

[34] W. Huang *et al.*, "Broadband terahertz half-wave plate with multi-layered metamaterials designed via quantum engineering," *J. Lightw. Technol.*, vol. 39, no. 24, pp. 7925–7929, Dec. 2021.

[35] Y. L. Li *et al.*, "Tunable ultra-broadband terahertz perfect absorber based on vanadium oxide metamaterial," *Opt. Exp.*, vol. 29, no. 25, pp. 41222–41233, Dec. 2021.

[36] N. Matthaiakakis, S. Droulias, and G. Kakarantzas, "Dynamic control of light chirality with nanostructured monolayer black phosphorus for broadband terahertz applications," *Adv. Opt. Mater.*, vol. 10, 2022, Art. no. 2102273.

[37] Y. Ren and B. Tang, "Switchable multi-functional VO_2-integrated metamaterial devices in the terahertz region," *J. Lightw. Technol.*, vol. 39, no. 18, pp. 5864–5868, Sep. 2021.

[38] M. Z. Jiang *et al.*, "Electrically triggered VO_2 reconfigurable metasurface for amplitude and phase modulation of terahertz wave," *J. Lightw. Technol.*, vol. 39, no. 11, pp. 3488–3494, Jun. 2021.

[39] J. D. Joannopoulos, P. R. Villeneuve, and S. H. Fan, "Photonic crystals: Putting a new twist on light," *Nature*, vol. 386, no. 6621, pp. 143–149, Mar. 1997.

[40] H. Han, H. Park, M. Cho, and J. Kim, "Terahertz pulse propagation in a plastic photonic crystal fiber," *Appl. Phys. Lett.*, vol. 80, no. 15, pp. 2634–2636, Apr. 2002.

[41] J. Dong *et al.*, "Versatile metal-wire waveguides for broadband terahertz signal processing and multiplexing," *Nat. Commun.*, vol. 13, 2022, Art. no. 741.

[42] V. A. Pogrebnyak *et al.*, "Non-Bragg reflections in a periodic waveguide," *Opt. Commun.*, vol. 232, no. 1–6, pp. 202–207, Mar. 2004.

[43] V. A. Pogrebnyak and E. P. Furlani, "Tunable bloch wave resonances and bloch gaps in uniform materials with reconfigurable boundary profiles," *Phys. Rev. Lett.*, vol. 116, 2016, Art. no. 206802.

[44] Z. Y. Tao *et al.*, "Wide forbidden band induced by the interference of different transverse acoustic standing-wave modes," *Appl. Phys. Lett.*, vol. 92, 2008, Art. no. 121920.

[45] Y. M. Xiao *et al.*, "Non-Bragg resonance of surface water waves in a trough with periodic walls," *Phys. Rev. E*, vol. 78, 2008, Art. no. 016311.

[46] B. Y. Ma *et al.*, "Slanted-eye featured forbidden bands in a water channel with undulated sidewalls," *Results Phys.*, vol. 22, 2021, Art. no. 103984.

[47] E. S. Lee, Y. B. Ji, and T. I. Jeon, "Terahertz band gap properties by using metal slits in tapered parallel-plate waveguides," *Appl. Phys. Lett.*, vol. 97, 2010, Art. no. 181112.